Quantum-information-theoretical measures to distinguish fermionized bosons from noninteracting fermions

Barnali Chakrabarti,[1,2] Arnaldo Gammal,[2] N. D. Chavda,[3] and Mantile Leslie Lekala[4]
[1]*Department of Physics, Presidency University, 86/1 College Street, Kolkata 700073, India*
[2]*Instituto de Física, Universidade de São Paulo, CEP 05508-090, São Paulo, Brazil*
[3]*Department of Applied Physics, Faculty of Technology and Engineering, The Maharaja Sayajirao University of Baroda, Vadodara-390001, India*
[4]*Department of Physics, University of South Africa, P. O. Box 392, Pretoria 0003, South Africa*

(Received 9 February 2024; revised 18 April 2024; accepted 2 May 2024; published 4 June 2024)

We study the dynamical fermionization of strongly interacting one-dimensional bosons in Tonks-Girardeau limit by solving the time-dependent many-boson Schrödinger equation numerically exactly. We establish that the one-body momentum distribution approaches the ideal Fermi gas distribution at the time of dynamical fermionization. The analysis is further complemented by the measures on the two-body level. The dynamical fermionization in the two-body level should be inferred as the presence of a distinct correlation hole along the diagonal of two-body correlation. Investigation of two-body momentum distribution for the strongly interacting bosons clearly exhibits a pattern along the diagonal which is not extinguished at the time of fermionization. Two-body local and nonlocal correlation also clearly distinguish the fermionized bosons from noninteracting fermions. The magnitude of distinguishablity between the two systems is further discussed employing suitable measures of information theory, i.e., the well-known Kullback-Leibler relative entropy and the Jensen-Shannon divergence entropy. We also observe very rich structure in the higher-body density for strongly correlated bosons, whereas noninteracting fermions do not possess any higher-order correlation beyond two-body.

DOI: 10.1103/PhysRevA.109.063308

I. INTRODUCTION

The one-dimensional (1D) gas of impenetrable bosons termed as Tonks-Girardeau (TG) gas corresponds to infinitely strong repulsive bosons in the Lieb-Liniger (LL) model [1,2]. The bosons interact through a contact potential. The physical properties of 1D bosons in the TG limit coincide with those of ideal Fermi gas in the same external potential. The properties determined by the square of the wave function such as the density profile and density-density correlation become identical with those of noninteracting fermions. It leads to the interesting manifestation of fermionization when the strongly interacting bosons escape their spatial overlap [3–8]. However, one-body density matrix and the momentum distribution are typically different from those of Fermi gas due to strong phase correlation originated from the bosonic statistics at the TG limit.

The dynamics of harmonically confined TG gas exhibits the more interesting scenario of "dynamical fermionization" during expansion on sudden release of the trap—the momentum distribution of TG gas evolves from bosonic to fermionic character. Some aspects of dynamical evolution of the TG gas have been theoretically studied [9–12]. Experimentally, optical confinement offers quasi-1D geometry and dynamical fermionization has recently been observed in the measure of asymptotic momentum distribution [13].

Despite a well-established understanding of dynamical fermionization, the topic still remains challenging as the work on higher-body density is highly limited [14]. The major existing calculations are based on the one-body level only. The aim of this work is to extend the calculation beyond one body in real as well as in momentum space and to understand whether fermionized bosons can really be distinguished from ideal Fermi gas. We try to resolve how one can infer the signature of dynamical fermionization in the higher-body level.

The dynamical evolution of quasi-1D harmonically trapped strongly interacting bosons in the TG limit is investigated in this work utilizing an *ab initio* many-body technique. We solve the many-bosons Schrödinger equation by using the multiconfigurational time-dependent Hartree method for indistinguishable particles (MCTDH-X), which calculates numerically exact many-body wave function [15–21]. Measures of many-body densities and correlation functions are of paramount interest to understand many-body physics. In such a strongly interacting regime we need very high orbitals to obtain the convergence in the many-body wave function. In the present work, dynamical evolution of $N = 5$ fermionized bosons is studied utilizing $M = 24$ orbitals in the computation of many-body wave function.

Our work is outlined as follows: (1) to explore the dynamical evolution of the fermionized bosons through the measures of x-space, k-space density and correlation in momentum space beyond one body, and (2) to apply information theoretic measures of relative entropy like nonsymmetric Kullback-Leibler, symmetric Kullback-Leibler, and the Jensen-Shannon divergence entropy for both one-body and two-body densities. The main aim is to justify that *when one-body measures of density, correlation, and relative entropies configure the*

dynamical fermionization, the corresponding measures on the two-body level are able to distinguish the noninteracting fermions and strongly interacting bosons at the time of fermionization determined from one-body measures.

Our observations are as follows: (1) As expected, dynamics of one-body densities in x space are identical between strongly interacting bosons and those of noninteracting fermions. (2) One-body k-space density exhibits that strongly interacting bosons attain fermionic character at a particular time, known as time for dynamical fermionization. (3) Measures of different relative entropies using one-body k density asymptotically approach to a constant value very close to zero at the time of fermionization. (4) Dynamics of the two-body x-space densities also exhibit the identical evolution for the two systems and cannot extract any additional physics. (5) However, two-body k-space density of strongly interacting bosons dynamically tends to approach the fermionic two-body k-space density, but remains distinctly different even at the time of fermionization. (6) Measures of local and nonlocal two-body correlation in the momentum space quantitatively estimate the difference between the two systems. (7) Measures of relative entropies utilizing two-body density in k space also clearly establish the distinct mutual information between the fermionized bosons and fermions on the two-body level. (8) We additionally analyze higher-body coherence. Fermions do not possess any higher-order correlation, whereas strongly interacting bosons exhibit rich structure in the three-body and four-body coherence.

All the above observations made from one-body measures uniquely confirm that the strongly interacting bosons at the TG limit dynamically acquire fermionic character at the time of dynamical fermionization. However, they can be distinguished on the basis of the corresponding two-body measures. Two-body correlation measures in k space are the key quantities to distinguish how the ferminozed bosons differ from ideal fermions *qualitatively*, whereas information theoretic measures of relative entropies *quantitatively* distinguish the two systems.

The paper is organized in the following way. Section II briefly describes the theoretical framework. We present dynamical measures in one-, two-, and higher-body levels in Sec. III, and a conclusion is made in Sec. IV.

II. THEORETICAL FRAMEWORK

In this section we introduce a brief description of the multiconfigurational time-dependent Hartree for bosons (MCTDHB), which is used to explore the dynamics. We also introduce the basic measures which are utilized to understand the many-body dynamics.

A. Many-body Hamiltonian wave function

The dynamical evolution of N bosons is governed by the time-dependent Schrödinger equation

$$H|\psi(t)\rangle = i\frac{\partial}{\partial t}|\psi(t)\rangle. \tag{1}$$

The full many-body Hamiltonian is

$$\hat{H}(x_1, x_2, \ldots x_N) = \sum_{i=1}^{N} \hat{h}(x_i) + \sum_{i<j=1}^{N} \hat{W}(x_i - x_j). \tag{2}$$

We used a dimensionless unit by dividing the Hamiltonian by $\frac{\hbar^2}{mL^2}$, where m is the mass of a boson and L is the length scale. In addition, $h(x) = -\frac{1}{2}\frac{\partial^2}{\partial x^2} + V(x)$ is the one-body Hamiltonian. $V(x)$ is the trapping potential, which is a harmonic potential for the present work. The interparticle interaction potential is $W(x_i - x_j) = \lambda\delta(x_i - x_j)$, where λ is the interaction strength.

In order to compute the time evolution of the many-body Schrödinger equation we use the MCTDHB, which employs variational time-adaptive orbitals in the expansion of the many-boson wave function. With an increase in the number of orbitals, it converges to the exact many-body Schrödinger results. In the MCTDHB method, time-dependent orbitals are used in the expansion of the field operator

$$\hat{\Psi}(x) = \sum_{j=1}^{M} \hat{b}_j(t)\phi_j(x,t). \tag{3}$$

Here, $\{\phi_j(x,t)\}$ is a complete orthonormal set of orbitals. $\hat{b}_j$ annihilates a boson in ϕ_j. This is in contrast with the full many-body Hamiltonian using time-independent orbitals, which require a large Fock space for convergence even for a few bosons. Introducing time-dependent orbitals, a faithful convergence can be achieved with a truncated number of orbitals. The orbitals are determined from the time-dependent variational principle [22–25]. When N bosons are distributed over M time-adaptive orbitals, the time-dependent many-boson function is taken as a linear combination of time-dependent permanents $|\bar{n};t\rangle$,

$$|\psi(t)\rangle = \sum_{\bar{n}} C_{\bar{n}}(t)|\bar{n};t\rangle. \tag{4}$$

In Eq. (4), the $\{C_{\bar{n}}(t)\}$ are the time-dependent expansion coefficients. The vector $\vec{n} = (n_1, n_2, \ldots, n_M)$ represents the occupation of the orbitals and $n_1 + n_2 + \cdots + n_M = N$, which preserves the total number of particles. In the second quantization representation, the permanents are given as

$$|\bar{n};t\rangle = \prod_{i=1}^{M}\left(\frac{[\hat{b}_i^{\dagger}(t)]^{n_i}}{\sqrt{n_i!}}\right)|vac\rangle. \tag{5}$$

In Eq. (4), the summation runs over all possible configurations and in the limit of $M \to \infty$, the set of permanents spans the complete Hilbert space and the expansion becomes exact. However, allowing time-dependent permanents, we use much shorter expansion, which leads to a significant computational advantage.

It is to be noted that both the coefficients $\{C_{\bar{n}}(t)\}$ and the orbitals $\{\phi_k(x,t)\}$ which comprise the permanents are independent parameters and are determined by the time-dependent variational principle. For the equations of motion governing the time evolution of $\{C_{\bar{n}}(t)\}$ and $\{\phi_k(x,t)\}$, we follow the variational principle based on the Lagrangian formulation [22]. Substituting the many-body ansatz into

the functional action of the time-dependent many-body Schrödinger equation leads to

$$S[\{C_{\bar{n}}(t)\},\{\phi_k(x,t)\}] = \int dt \left\{ \langle\Psi(t)|\hat{H} - i\frac{\partial}{\partial t}|\Psi(t)\rangle - \sum_{k,j=1}^{M} \mu_{kj}(t)[\langle\phi_k|\phi_j\rangle - \delta_{kj}] \right\}. \quad (6)$$

Next, stationarity of the action with respect to the independent variations of $\{C_{\bar{n}}(t)\}$ and $\{\phi_j(x,t)\}$ are required. $\{\mu_{kj}(t)\}$ are time-dependent Lagrange multipliers which guarantee the orthonormality of the orbitals during time propagation.

It is to be noted that the use of optimized time-dependent orbitals leads to very fast convergence in the simulation compared to the many-body Schrödinger equation with time-independent orbitals, and a given degree of accuracy is reached with much shorter expansion [26,27]. We also emphasize that MCTDHB is more accurate than exact diagonalization, which uses the finite basis and is not optimized. In contrast, in MCTDHB, as we use a time-adaptive many-body basis set, it can dynamically follow the building correlation due to interparticle interaction [17,18,28,29]. It is already established as a very efficient many-body method and used for different trap geometry and range of interparticle interaction [30–33]. The MCTDHB method and the algorithm have been cast into a software package [34,35].

B. Quantities of interest

1. One-body and higher-order densities

(i) The reduced one-body density matrix in coordinate space is defined as

$$\rho^{(1)}(x_1'|x_1;t) = N\int dx_2\, dx_3 ... dx_N\, \psi^*(x_1', x_2, \ldots, x_N;t) \times \psi(x_1, x_2, \ldots, x_N;t). \quad (7)$$

Its diagonal gives the one-body density $\rho(x,t)$, defined as

$$\rho(x;t) = \rho^{(1)}(x_1' = x|x_1 = x;t). \quad (8)$$

(ii) The pth-order reduced density matrix in coordinate space is defined by

$$\rho^{(p)}(x_1', \ldots, x_p'|x_1, \ldots, x_p;t) = \frac{N!}{(N-p)!}\int dx_{p+1} ... dx_N \psi^*(x_1', \ldots, x_p', x_{p+1}, \ldots, x_N;t) \times \psi(x_1, \ldots, x_p, x_{p+1} \ldots, x_N;t). \quad (9)$$

The diagonal of p-body density can be represented as

$$\rho^{(p)}(x_1, \ldots, x_p;t) = \langle\psi(t)|\hat{\psi}^\dagger(x_1)\ldots\hat{\psi}^\dagger(x_p)\hat{\psi}(x_p) \times \ldots\hat{\psi}(x_1)|\psi(t)\rangle. \quad (10)$$

It provides the p-particle density distribution at time t.

To calculate the density in momentum space, one needs to follow the prescription provided in Ref. [36]. Introducing p D-dimensional Fourier transform to r_i and r_i', one arrives at

$$\rho^{(p)}(k_1, ..., k_p|k_1', ..., k_p';t) = \sum_i n_i^{(p)}(t)\alpha_i^{(p)}(k_1, ..., k_p, t)\alpha_i^{(p)*}(k_1', ..., k_p', t), \quad (11)$$

where $n_i^{(p)}(t)$ is the ith eigenvalue of the pth-order reduced density matrix and $\alpha_i^{(p)}(k_1, ..., k_p, t)$ the corresponding eigenfunction. The eigenfunctions are known as natural p functions and the eigenvalues as natural occupations.

2. Glauber correlation function

The normalized pth-order Glauber correlation function would be the most important quantity to measure the spatial coherence. It is defined as

$$g^{(p)}(x_1', \ldots, x_p', x_1, \ldots, x_p;t) = \frac{\rho^{(p)}(x_1, \ldots, x_p|x_1', \ldots, x_p';t)}{\sqrt{\Pi_{i=1}^p \rho^{(1)}(x_i|x_i;t)\rho^{(1)}(x_i'|x_i';t)}}. \quad (12)$$

The diagonal of $g^{(p)}(x_1', \ldots, x_p', x_1, \ldots, x_p;t)$ gives a measure of pth-order coherence and is calculated as

$$g^{(p)}(x_1, \ldots, x_p;t) = \frac{\rho^{(p)}(x_1, \ldots, x_p;t)}{\Pi_{i=1}^p|\rho^{(1)}(x_i)|}. \quad (13)$$

If $|g^{(p)}(x_1, \ldots, x_p;t)| = 1$, the system is fully coherent, otherwise the state is only partially coherent. When $g^{(p)}(x_1, \ldots, x_p;t) > 1$, the detection probabilities at positions $x_1, \ldots, x_p$ are correlated and $g^{(p)}(x_1, \ldots, x_p;t) < 1$ are anticorrelated. Equation (13) is further utilized to calculate the local two-particle correlation $g^{(2)}(0,0)$ and nonlocal two-particle correlation $g^{(2)}(0,x)$.

The pth-order correlation function in momentum space is given by

$$g^{(p)}(k_1', \ldots, k_p', k_1, \ldots, k_p;t) = \frac{\rho^{(p)}(k_1, \ldots, k_p|k_1', \ldots, k_p';t)}{\sqrt{\Pi_{i=1}^p \rho^{(1)}(k_i|k_i;t)\rho^{(1)}(k_i'|k_i';t)}}. \quad (14)$$

The diagonal of $g^{(p)}(k_1', \ldots, k_p', k_1, \ldots, k_p;t)$ measures the pth-order coherence in the momentum space. For values $g^{(p)}(k_1, \ldots, k_p;t) > 1$, the detection probabilities at positions $k_1, \ldots, k_p$ are correlated, and $g^{(p)}(k_1, \ldots, k_p;t) < 1$ correspond to loss of coherence and are anticorrelated. Equation (14) is further utilized to calculate the local two-particle correlation $g^{(2)}(0,0)$ and nonlocal two-particle correlation $g^{(2)}(0,k)$.

3. Information distance measures

Shannon entropy and Fisher information are considered as the key measures to exhibit higher-order characteristics in position and momentum space density distribution and have been extensively utilized in atomic systems [37–43]. However, to measure the difference between two probability distributions over the same variable, a measure called Kullback-Leibler (KL) relative entropy is the ideal quantity [44–46]. Relative entropy provides mutual information

between two probability distributions of the same order and defined in the same space. KL relative entropy in x space is measured as

$$K(t) = \int \rho_1^{(1)}(x,t) \ln \frac{\rho_1^{(1)}(x,t)}{\rho_2^{(1)}(x,t)}\, dx, \tag{15}$$

where $\rho_1^{(1)}$ and $\rho_2^{(1)}$ are the one-body densities for two different systems described in the same space and they are calculated using $\rho^{(1)}(x,t) = \langle\psi(t)|\hat{\psi}^\dagger(x)\hat{\psi}(x)|\psi(t)\rangle$.

Thus, the measure of K can be interpreted as a measure of deviation of $\rho_1^{(1)}$ from $\rho_2^{(1)}$, i.e., to estimate how the two systems are identical or close or far apart. Thus, for any distributions $\rho_1^{(1)}$ and $\rho_2^{(1)}$, $K \geqslant 0$. However, it is a nonsymmetric measure as it depends on which distribution is considered as "reference" and which is considered as "comparison" distribution. The symmetrized Kullback distance SK is defined as [47]

$$SK(t) = \int \rho_1^{(1)}(x,t) \ln \frac{\rho_1^{(1)}(x,t)}{\rho_2^{(1)}(x,t)}\, dx + \int \rho_2^{(1)}(x,t) \ln \frac{\rho_2^{(1)}(x,t)}{\rho_1^{(1)}(x,t)}\, dx. \tag{16}$$

The physical meaning of SK distance is very clear. SK is zero for two identical species and approaches to a large value as the difference between the one-body densities of two systems $\rho_1^{(1)}$ and $\rho_2^{(1)}$ increases. Another symmetrized measure of relative entropy is the Jensen-Shannon divergence entropy as [48,49]

$$J(t) = -\int \left(\frac{\rho_1^{(1)}(x,t) + \rho_2^{(1)}(x,t)}{2}\right) \times \ln\left(\frac{\rho_1^{(1)}(x,t) + \rho_2^{(1)}(x,t)}{2}\right) dx + \frac{1}{2}\int \rho_1^{(1)}(x,t) \ln \rho_1^{(1)}(x,t)\, dx + \frac{1}{2}\int \rho_2^{(1)}(x,t) \ln \rho_2^{(1)}(x,t)\, dx. \tag{17}$$

Both the measures of SK and J are symmetrized and compare two probability distributions regardless of which distribution is considered as the reference and which is considered as the comparison distribution. For two indistinguishable densities K and SK should settle to zero, whereas J should settle to a small constant value. In contrast, for two distinguishable densities, K, SK, and J can be significantly high. The corresponding definitions of K, SK, and J measures in k space are

$$K(t) = \int \rho_1^{(1)}(k,t) \ln \frac{\rho_1^{(1)}(k,t)}{\rho_2^{(1)}(k,t)}\, dk \tag{18}$$

$$SK(t) = \int \rho_1^{(1)}(k,t) \ln \frac{\rho_1^{(1)}(k,t)}{\rho_2^{(1)}(k,t)} dk + \int \rho_2^{(1)}(k,t) \ln \frac{\rho_2^{(1)}(k,t)}{\rho_1^{(1)}(k,t)}\, dk \tag{19}$$

$$J(t) = -\int \left(\frac{\rho_1^{(1)}(k,t) + \rho_2^{(1)}(k,t)}{2}\right) \times \ln\left(\frac{\rho_1^{(1)}(k,t) + \rho_2^{(1)}(k,t)}{2}\right) dk + \frac{1}{2}\int \rho_1^{(1)}(k,t) \ln \rho_1^{(1)}(k,t)\, dk + \frac{1}{2}\int \rho_2^{(1)}(k,t) \ln \rho_2^{(1)}(k,t)\, dk, \tag{20}$$

where one-body density in k space $\rho^{(1)}(k,t)$ is calculated using $\rho^{(1)}(k,t) = \langle\psi(t)|\hat{\psi}^\dagger(k)\hat{\psi}(k)|\psi(t)\rangle$.

However, it is also interesting to have measures of the above three distributions using two-body density in x space $\rho^{(2)}(x_1,x_2,t) = \langle\psi(t)|\hat{\psi}^\dagger(x_1)\hat{\psi}^\dagger(x_2)\hat{\psi}(x_1)\hat{\psi}(x_2)|\psi(t)\rangle$.

The corresponding measures of K, SK, and J in x space are defined through

$$K(t) = \int \rho_1^{(2)}(x_1,x_2,t) \ln \frac{\rho_1^{(2)}(x_1,x_2,t)}{\rho_2^{(2)}(x_1,x_2,t)}\, dx_1\, dx_2, \tag{21}$$

where $\rho_1^{(2)}$ and $\rho_2^{(2)}$ correspond to two-body densities of the two different systems but described in the same space. It will facilitate to understand whether the two systems are close in the measure of two-body perspective. The corresponding definitions of SK and J in x space are as follows:

$$SK(t) = \int \rho_1^{(2)}(x_1,x_2,t) \ln \frac{\rho_1^{(2)}(x_1,x_2,t)}{\rho_2^{(2)}(x_1,x_2,t)} dx_1 dx_2 + \int \rho_2^{(2)}(x_1,x_2,t) \ln \frac{\rho_2^{(2)}(x_1,x_2,t)}{\rho_1^{(2)}(x_1,x_2,t)}\, dx_1\, dx_2 \tag{22}$$

$$J(t) = -\int \left(\frac{\rho_1^{(2)}(x_1,x_2,t) + \rho_2^{(2)}(x_1,x_2,t)}{2}\right) \times \ln\left(\frac{\rho_1^{(2)}(x_1,x_2,t) + \rho_2^{(2)}(x_1,x_2,t)}{2}\right) dx_1\, dx_2 + \frac{1}{2}\int \rho_1^{(2)}(x_1,x_2,t) \ln \rho_1^{(2)}(x_1,x_2,t)\, dx_1\, dx_2 + \frac{1}{2}\int \rho_2^{(2)}(x_1,x_2,t) \ln \rho_2^{(2)}(x_1,x_2,t)\, dx_1\, dx_2. \tag{23}$$

Defining two-body density in k space as $\rho^{(2)}(k_1,k_2,t) = \langle\psi(t)|\hat{\psi}^\dagger(k_1)\hat{\psi}^\dagger(k_2)\hat{\psi}(k_1)\hat{\psi}(k_2)|\psi(t)\rangle$, we can have the measures of S, SK, and J in momentum space from the two-body perspective. They are calculated as

$$K(t) = \int \rho_1^{(2)}(k_1,k_2,t) \ln \frac{\rho_1^{(2)}(k_1,k_2,t)}{\rho_2^{(2)}(k_1,k_2,t)}\, dk_1\, dk_2 \tag{24}$$

$$SK(t) = \int \rho_1^{(2)}(k_1,k_2,t) \ln \frac{\rho_1^{(2)}(k_1,k_2,t)}{\rho_2^{(2)}(k_1,k_2,t)} dk_1 dk_2 + \int \rho_2^{(2)}(k_1,k_2,t) \ln \frac{\rho_2^{(2)}(k_1,k_2,t)}{\rho_1^{(2)}(k_1,k_2,t)}\, dk_1\, dk_2 \tag{25}$$

$$J(t) = -\int \left(\frac{\rho_1^{(2)}(k_1,k_2,t) + \rho_2^{(2)}(k_1,k_2,t)}{2} \right) \times \ln \left(\frac{\rho_1^{(2)}(k_1,k_2,t) + \rho_2^{(2)}(k_1,k_2,t)}{2} \right) dk_1\, dk_2 + \frac{1}{2}\int \rho_1^{(2)}(k_1,k_2,t) \ln \rho_1^{(2)}(k_1,k_2,t)\, dk_1\, dk_2 + \frac{1}{2}\int \rho_2^{(2)}(k_1,k_2,t) \ln \rho_2^{(2)}(k_1,k_2,t)\, dk_1\, dk_2. \quad (26)$$

III. RESULTS OF EXPANSION DYNAMICS

A. Measures on one-body level

We choose $N = 5$ strongly interacting bosons with $\lambda = 25$, in the harmonic oscillator trap $V(x) = \frac{1}{2}x^2$. We use MCTDHB for bosons and for the noninteracting fermions we use multiconfigurational time-dependent Hartree for fermions (MCTDHF) implemented in the MCTDH-X software package [35]. The computation is done with $M = 24$ orbitals for strongly interacting bosons, and the convergence is assured as the last orbital occupation is insignificant. For noninteracting fermions, computation is done with $M = 5$ orbitals, where each orbital has an exactly equal contribution of 20% population. The initial state is prepared at the ground state in the harmonic oscillator and the 1D expansion is studied on sudden removal of the trap. In Fig. 1, we plot the momentum distribution of the expanding bosons at various times and compared with the fermionic limit. The initial bosonic distribution gradually develops fermionic character and finally settles to five humps at time $t = 8.0$, which is chosen as the time for dynamical fermionization. Figure 1 can also be compared with Fig. 1 of Ref. [9]. We extend simulation till the time $t = 10.0$ (up to $t = 10.0$, we are able to present fully converged results) and observe that fermionic properties of the interacting bosons are maintained. In Fig. 2, we plot the time-evolving density both in the real space as well as in the momentum space. The expansion in x space clearly exhibits the propagation of five independent jets, signifying expansion of five strongly interacting bosons, whereas the momentum density exhibits gradual development of five humps which settle at time $t = 8.0$ and remain unchanged till time $t = 10.0$.

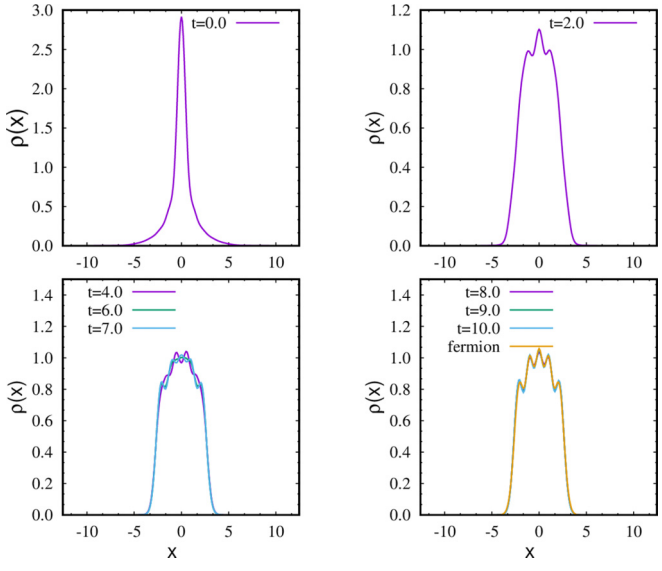

FIG. 1. Momentum distribution of expanding strongly interacting bosons at different times as indicated on the panels. Computation is done for $N = 5$ strongly interacting bosons with interaction strength $\lambda = 25$ and using $M = 24$ orbitals. Comparison is made for the dynamics of $N = 5$ noninteracting fermions, and computation is made with $M = 5$ orbitals.

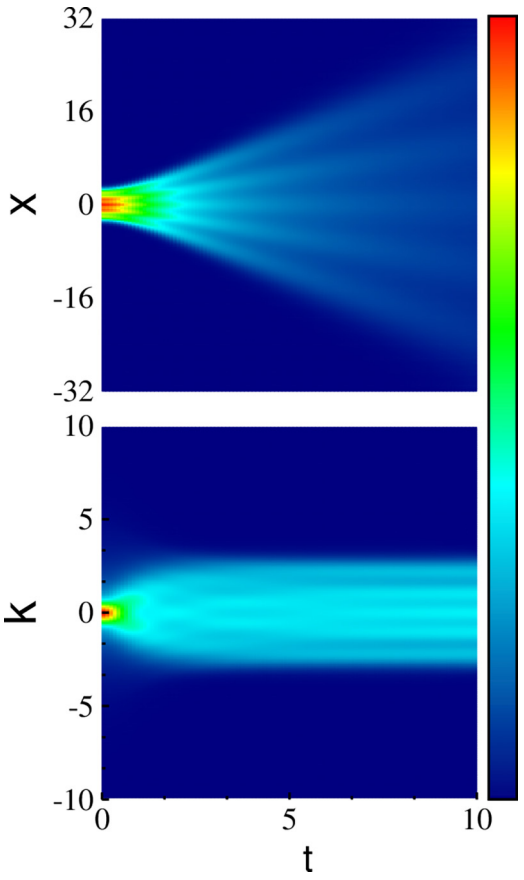

FIG. 2. The time evolution of the density profile during the expansion of five strongly interacting bosons initially trapped in a harmonic oscillator (HO) potential and suddenly released. The top panel corresponds to real space, x density, and the bottom panel corresponds to momentum space, k density. Computation is done with $M = 24$ orbitals and chosen interaction strength $\lambda = 25$. When the x density exhibits the expansion with distinct many-body features, k density exhibits the asymptotic approach to fermionic limit.

Figure 3 depicts a comparison of dynamical evolution of reduced one-body density in x space $\rho^{(1)}(x, x')$ between the strongly interacting bosons (left panel) and noninteracting fermions (right panel), exhibiting identical expansion dynamics. Initially at ($t = 0$), the density is clustered at the center due to the harmonic trap, but becomes flatter and broader with an increase in time. The density gradually acquires modulations and the number of humps tries to saturate to the number of bosons. At $t = 8.0$, we observe the emergence of five distinct humps. The hump at the center is the brightest

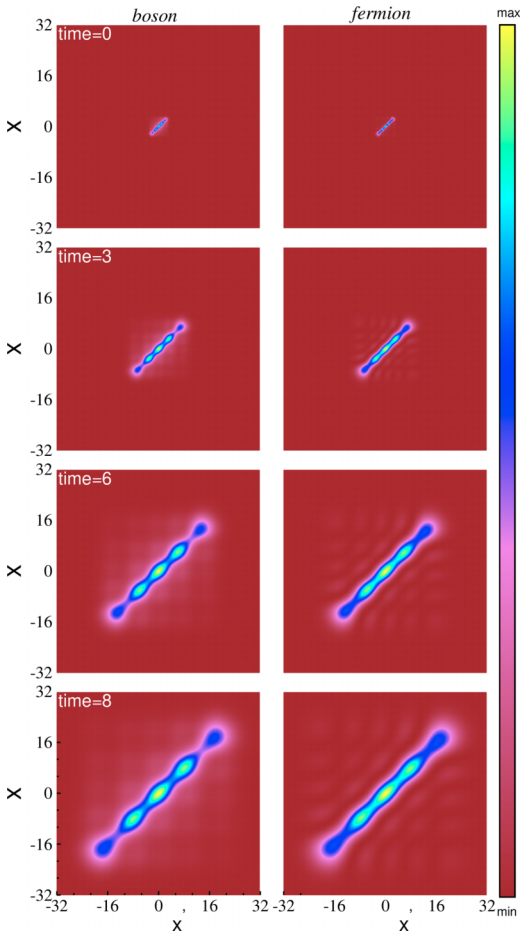

FIG. 3. Snapshots of the time evolution of reduced one-body density in the x space $[\rho^{(1)}(x, x')]$ during the expansion of $N = 5$ strongly interacting bosons with interaction strength $\lambda = 25$ are presented (left panel). Computation is done with $M = 24$ orbitals. Comparison is made for the dynamics of noninteracting fermions in the right panel, and computation is made with $M = 5$ orbitals. The dynamical evolution of the two systems is identical in x space.

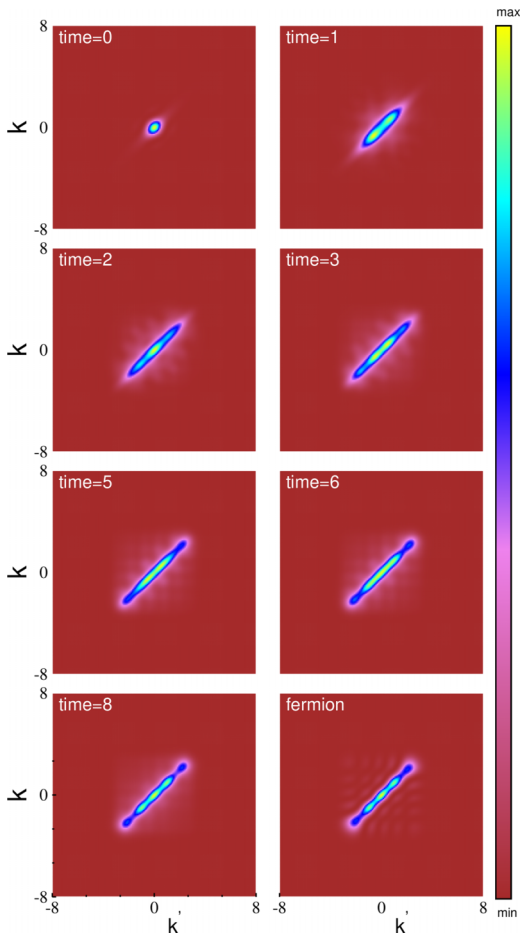

FIG. 4. Snapshots of the time evolution of reduced one-body density in the k space $[\rho^{(1)}(k, k')]$ during the expansion of $N = 5$ strongly interacting bosons with interaction strength $\lambda = 25$ are presented for different times. Computation is done with $M = 24$ orbitals. Comparison is made with fermionic momentum density distribution (last panel on the right side), and computation is made with $M = 5$ orbitals. At time $t = 8.0$, strongly interacting bosons attain the fermionic density distribution.

where the potential was initially zero, the two outer humps are less pronounced due to the initial nonzero confining potential, and the two outermost humps are least pronounced which are away from the center. It is clearly seen that both strongly interacting bosons and noninteracting fermions exhibit identical expansion dynamics in x space. We additionally note that the density's maxima in the TG regime are distinct but not isolated, and the five bright spots are interconnected. Next, we study the expansion dynamics through reduced one-body density in k space, i.e., $\rho^{(1)}(k, k')$, which evaluates the time for dynamical fermionization. Figure 4 describes the momentum distribution of the expanding gas with five bosons at different times ($t = 0, 1, 2, 3, 5, 6, 8$). Initially at $t = 0$, the density is in cluster form at the center of the trap; with time it gradually develops peaks, the peaks become prominent, and finally become identical with the fermionic density distribution (last panel on the right side) at $t = 8.0$. We observe dynamical fermionization occurs as the momentum distribution approaches ideal Fermi distribution at time $t = 8.0$. It is not possible to distinguish the fermionized bosons and the ideal fermions from the measure of one-body k density. We conclude $t = 8.0$ is the time for dynamical fermionization for the present system.

We calculate the measures of relative entropies K, SK, and J in the x space using Eqs. (15), (16), and (17), respectively. However, as shown in Fig. 3, as the fermionized bosons and noninteracting fermions exhibit identical one-body expansion dynamics in real space, the corresponding relative entropy measures are identically zero all throughout the dynamical evolution. The corresponding measures in momentum space as determined by Eqs. (18)–(20) are plotted in Fig. 5 till time $t = 10.0$. All the measures have the same trend and conclude the same physics. K and SK are very close and J lies below. We find initially that the values are significant, which infers that for the two systems, strongly interacting bosons and fermions are different. With time, all three measures gradually decrease, which signifies that the strongly interacting bosons gradually attain the fermionic characteristics. Finally, at the time of fermionization ($t = 8.0$), they asymptotically settle to

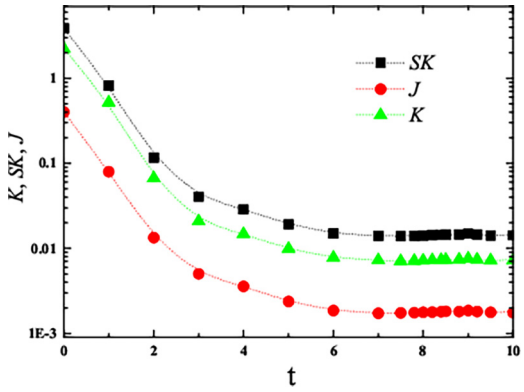

FIG. 5. Dynamics of relative entropy measures K, SK, and J in momentum space as determined by Eqs. (18), (19), and (20) respectively. The corresponding one-body momentum density is utilized to evaluate the entropy measures. All the measures exhibit how the strongly interacting bosons asymptotically approach the fermionization limit at time $t = 8.0$ when all the relative entropy measures reach a very small value.

a very small but nonzero constant value, which signifies that the density of the two systems becomes indistinguishable. The limiting value is not zero due to logarithmic terms present in the integration. A very minute difference can contribute significantly. We have investigated carefully the time zone [8, 10] and we observe the relative entropy measures settle to the limiting value only.

All the measures based on the dynamics of one-body density support the well-accepted fact that at the time of fermionization the strongly correlated bosons asymptotically achieve fermionization. The one-body momentum densities of the two systems become indistinguishable. However, it needs to be examined whether the same conclusion can be made from the measures using two-body densities.

B. Measures on two-body level

We discuss dynamics of the reduced two-body density in x space $\rho^{(2)}(x, x')$ in Fig. 6. Comparison between strongly interacting bosons and noninteracting fermions are presented at the same time scale as of one-body density (Fig. 3). The left panel corresponds to the strongly interacting bosons and the right panel corresponds to the noninteracting fermions. Initially, the atoms are clustered near the center ($x = x' = 0$) for both the cases of interacting bosons and noninteracting fermions. With time, $\rho^{(2)}$ gradually spreads out to the off-diagonal ($x \neq x'$). The diagonal ($x \simeq x'$) is gradually depleted and a so-called "correlation hole" forms on the diagonal. Thus, the bosons gradually overcome their spatial overlap; the probability of finding two bosons at the same position tends toward zero. With time, the correlation hole spreads and finally converges in the fermionization limit at time $t = 8.0$. Off-diagonal spreading also converges in the fermionization time. Similar to the one-body density, the maxima which are formed across the off-diagonal are distinct but not isolated. We infer that the correlation hole along the diagonal and the confined spreading at the time of fermionization are the unique signatures of the two-body density of a dynamically

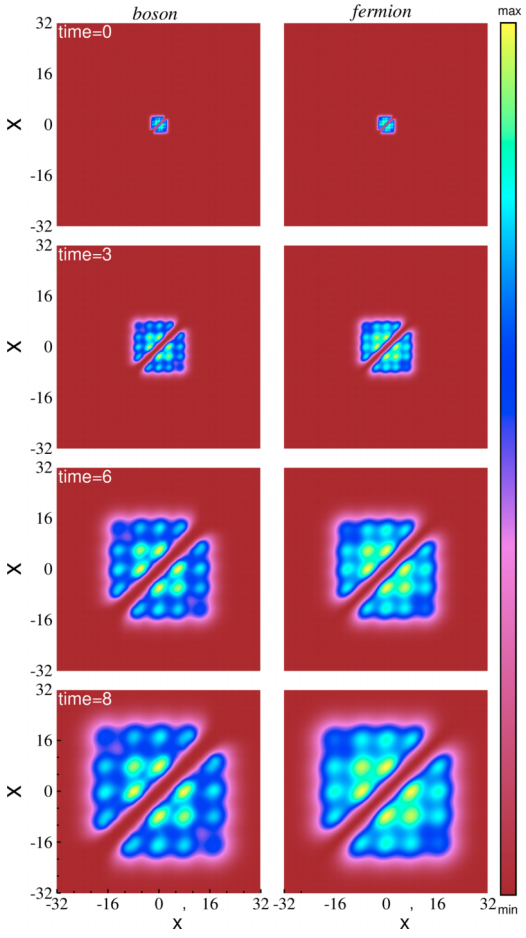

FIG. 6. Snapshots of the time evolution of reduced two-body density in x space $[\rho^{(2)}(x, x')]$ during the expansion of $N = 5$ strongly interacting bosons with interaction strength $\lambda = 25$ are presented (left panel). Computation is done with $M = 24$ orbitals. Comparison is made with dynamics of expansion for noninteracting fermions with $M = 5$ orbitals (right panel). Identical evolution of the two systems is observed.

evolved fermionized state. The dynamics exhibited by the noninteracting fermions is exactly identical to that of interacting bosons.

In Fig. 7, we plot the reduced two-body density in k space $\rho^{(2)}(k, k')$ for the same time points as chosen for Fig. 4. Initially, at time $t = 0$, we observe the density in the clustered state at the center. With time $\rho^{(2)}$ spreads out to the off-diagonal and the diagonal is depleted. However, no distinct correlation hole is created, and the strongly interacting bosons try to make a diagonal gap, but some internal structure along the diagonal exist. $\rho^{(2)}(k, k')$ remains localized near $k \leqslant 3.5$, because of the finite energy. The well-defined bright spot indicates the localization of the bosons in momentum space. With further time evolution the internal structure along the diagonal is greatly reduced but not completely extinguished like ideal fermionic two-body reduced momentum distribution. We infer that the distinct correlation hole and the complete extinction of diagonal correlation are the unique signatures of fermionization at the two-body level. Thus, we are unable

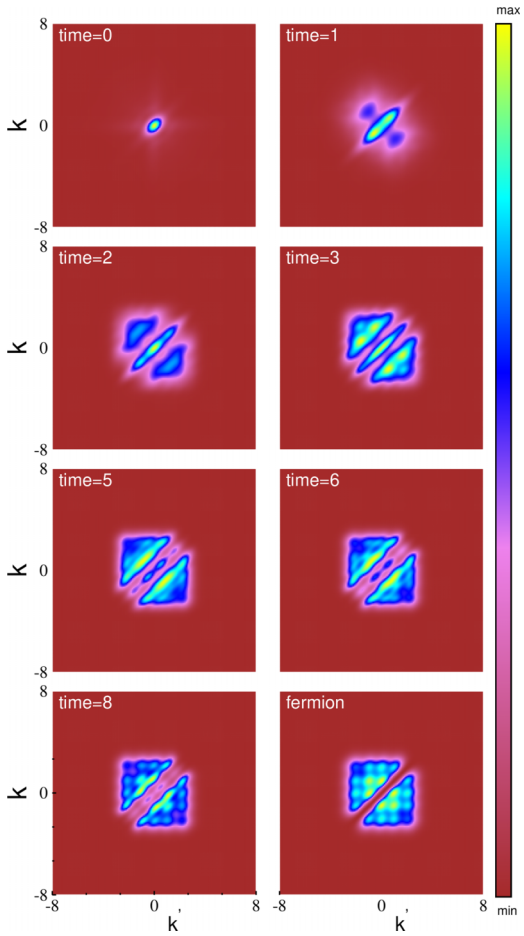

FIG. 7. Snapshots of the time evolution of the reduced two-body momentum density $[\rho^{(2)}(k,k')]$ during the expansion of $N=5$ strongly interacting bosons with interaction strength $\lambda=25$ and orbitals $M=25$ are presented for different times. The corresponding fermionic distribution computed with $M=5$ is presented in the last panel on the right side. The strongly interacting bosons, which were initially at the center of the trap, gradually develop a very weak correlation hole along the diagonal. However, at the time of dynamical fermionization, the correlation width and intensity strongly differ from the distinct correlation hole in the fermionic distribution.

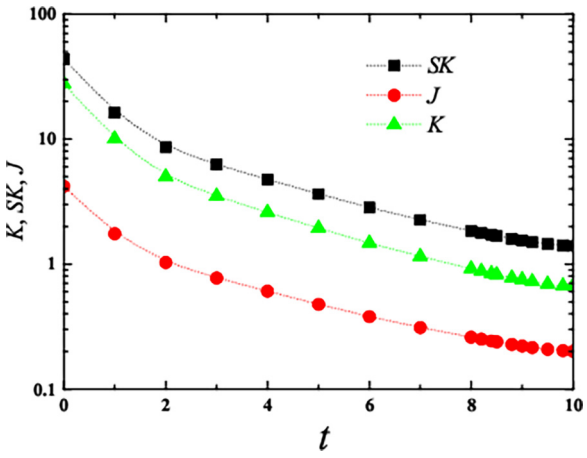

FIG. 8. Dynamics of relative entropy measures between the strongly interacting bosons and the ideal fermions using two-body momentum density in Eqs. (24)–(26). The initial large value clearly signifies how the two systems are quite far from each other. With time all three measures gradually decrease as the strongly interacting bosons try to acquire fermionic distribution. However, unlike the observation made in Fig. 5, K, SK, and J smoothly decrease.

to locate the signature of dynamical fermionization in the two-body level.

To understand qualitatively how close the strongly interacting bosons feature the fermionic properties in the two-body level, we utilize the information distance measures. The measures utilizing two-body densities in x space from Eqs. (21)–(23) reduce to zero as the fermionized bosons and noninteracting fermions exhibit indistinguishable expansion dynamics as shown in Fig. 6. The corresponding measures utilizing two-body momentum density from Eqs. (24)–(26) are plotted in Fig. 8. The initial large value in all the relative entropy measures clearly distinguishes that a strongly interacting boson's density is completely different from that of fermionic two-body density. With the increase in time, the entropy measures continuously fall, which signifies that the two-body density of bosons try to achieve fermionic two-body density. At the time of fermionization ($t=8.0$), all the measures have significant value far above zero, leading to infer that dynamically fermionized bosons have distinguishable density from that of noninteracting fermions in the two-body level. It signifies that, although at the time of fermionization the one-body density of strongly interacting bosons becomes identical to that of ideal fermions, their corresponding two-body density differs.

We also summarize some quantitative measures at the time of fermionization. The one-body k entropy is evaluated by $S_k^{1B}=\int dk\rho^{(1)}(k,t)\ln[\rho^{(1)}(k,t)]$ and the two-body k entropy is evaluated by $S_k^{2B}=\int dk_1dk_2\rho^{(2)}(k_1,k_2;t)\ln[\rho^{(2)}(k_1,k_2;t)]$. At the time of fermionization ($t=8.0$), $S_k^{1B}=1.830$ for strongly interacting bosons, which is closely comparable with 1.819 for noninteracting fermions. The corresponding relative entropy measures in the one-body level are $K=0.007$, $SK=0.014$, and $J=0.001$. In contrast, for two-body k entropy for interacting bosons, $S_k^{2B}=93.985$; this is significantly different from 10.523, which is the two-body k entropy for noninteracting fermions. The corresponding relative entropy measures are $K=0.919$, $SK=1.850$, and $J=0.260$, which clearly signify that there is no signature of dynamical fermionization on the two-body aspects.

To estimate further the difference between the strongly interacting bosons and the fermions, we calculate the local two-body correlation function in both x and k space. From Fig. 6, it is clearly seen that the two-body correlation is completely extinguished at $x=x'=0$ all throughout the dynamics for both the fermionized bosons and noninteracting fermions, which leads to $g^{(2)}(x=0,x'=0)=0$ as calculated from Eq. (13). However, in the k space, the local two-body correlation $g^{(2)}(k=0,k'=0)$ would contain significant quantitative information about the close proximity of the two systems in the entire dynamics. From Eq. (14) we calculate $g^{(2)}(k=0,k'=0)$ for the fermionized bosons and plot it in Fig. 9. It is expected that for fermions $g^{(2)}(0,0)$ is uniquely zero, which is the typical feature of

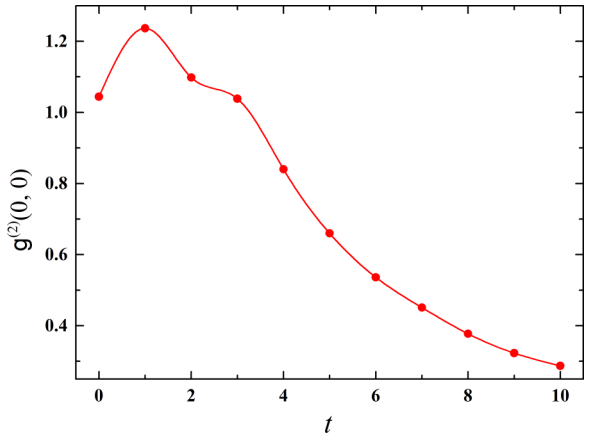

FIG. 9. The time evolution of the local two-body correlation $g^{(2)}(0,0)$ for the strongly interacting bosons in momentum space. $g^{(2)}(0,0) = 0$ corresponds to fermionization limit, which infers the existence of a distinct correlation hole; two-body correlation is completely extinguished. Strongly interacting bosons initially have strong local correlation; it dies with time but does not reach zero at the time of fermionization.

fermionization on the two-body level. For strongly interacting bosons it starts from $g^{(2)}(0,0) = 1.0$, and then after a small increase, it smoothly decreases. However, at the time of fermionization (determined from one-body measures), it reaches to $g^{(2)} = 0.4$ but does not settle and smoothly decreases. It indicates that for strongly interacting bosons the local two-body correlation is not completely extinguished, which helps to identify strongly interacting bosons from noninteracting fermions. The corresponding two-body nonlocal correlation $g^{(2)}(0,k)$ is plotted in Fig. 10. Strongly interacting bosons reach to the no-correlation limit with some initial characteristic oscillation. However, the fermions attain the no-correlation limit sharply and do not exhibit any resolvable dynamical structure.

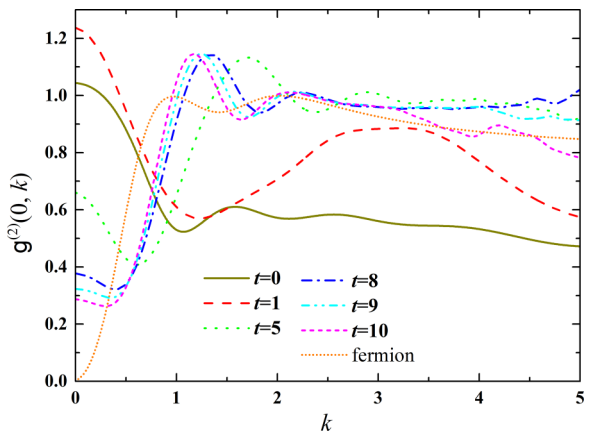

FIG. 10. The time evolution of two-body nonlocal correlation $g^{(2)}(0,k)$ for the strongly interacting bosons. $g^{(2)}(0,k) \to 1$ implies the no-correlation limit, which is achieved at the characteristic time of fermionization. We also observe some peculiar oscillation around the no-correlation zone for the strongly interacting bosons.

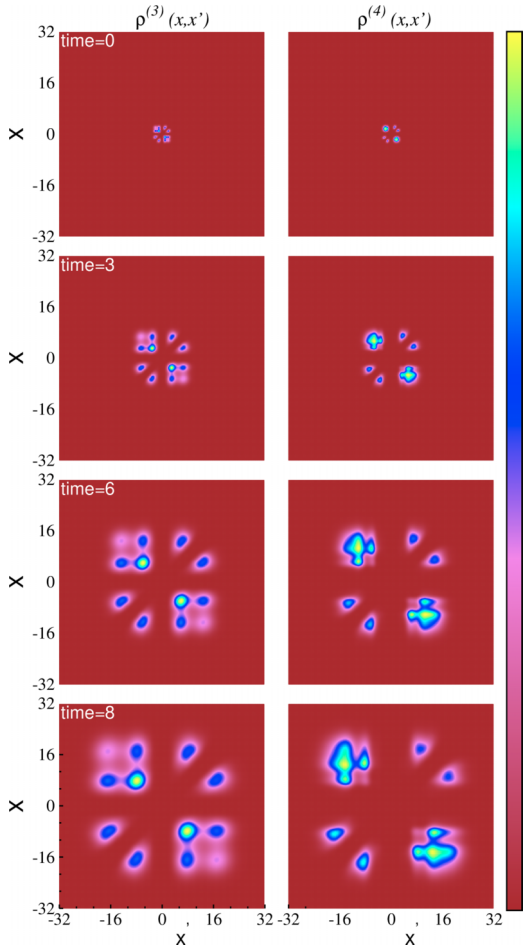

FIG. 11. Snapshots of the dynamics of three-body density $\rho^{(3)}(x,x')$ (left column) and $\rho^{(4)}(x,x')$ (right column) for $N = 5$ strongly interacting bosons. See the text for details.

C. Higher-order coherence

Figures 11 and 12 depict the higher-order densities $\rho^{(p)}(p = 3, 4)$ in x and k space for the strongly interacting bosons; the noninteracting fermions do not exhibit any higher-order correlation beyond two-body. The $\rho^{(p)}$ provides the probability of detecting particles at x and x' when the remaining $p-2$ particles are fixed at some reference positions. For fermionized bosons, the diagonal of the high-order p-body densities $\rho^{(p)}(x,x)$ vanishes as the so-called correlation hole results from the strong interaction strength that mimics the Pauli principle, preventing finding two bosons at the same position. The maxima exhibit a well-defined peaked structure which indicates the localization of the atoms in position space. The maxima along the antidiagonal $x = -x'$ infers that the bosons maximize the distance between each other, whereas the maxima along the subdiagonal infers that the bosons minimize the potential energy. The additional correlation holes appear at the fixed values of the remaining $p-2$ coordinates of $\rho^{(p)}$, preventing finding other bosons at these positions.

In Fig. 11, we plot three-body density $\rho^{(3)}(x,x')$ (keeping the third particle at the fixed reference point $x_3 = 0$) at the left column and four-body density $\rho^{(4)}(x,x')$ (keeping the third and the fourth particle at the fixed reference points $x_3 = 0$ and

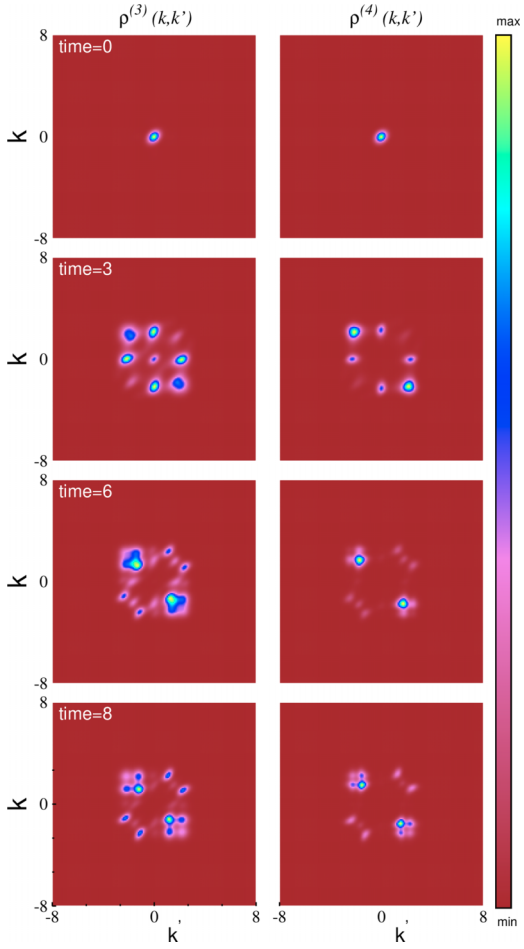

FIG. 12. Snapshots of the dynamics of three-body density $\rho^{(3)}(k, k')$ (left column) and $\rho^{(4)}(k, k')$ for $N = 5$ strongly interacting bosons. See the text for details.

$x_4 = 0.47$) at the right column. Initially both three-body and four-body densities are localized at the center. With time, the maxima is developed along the antidiagonal as well as along the subdiagonal. Additional correlation holes also appear at the fixed reference points as the probability of finding other bosons at these positions is zero. The three-body correlation structure exhibits further delocalization as expected, and finally converges at the time of dynamical fermionization. The corresponding three-body and four-body densities in the momentum space are plotted in Fig. 12. Like Fig. 11, it also exhibits a rich dynamical structure.

IV. CONCLUSION

For the strongly interacting TG limit, the wave function of the interacting bosons in one dimension maps to that of noninteracting fermions. The properties of the two systems which are determined by the amplitude of the wave function are identical, whereas the measurement in the momentum space exhibits dynamical fermionization. This conclusion is established on the basis of one-body analysis. In this work we extend the measure to higher-order densities and correlation function using numerically exact solution of the time-dependent many-boson Schrödinger equation. We establish all the existing physics and additionally include the measures of three different kinds of relative entropies which utilize the one-body in the momentum space. We clearly find that all the measures on the one-body level unambiguously establish the onset of fermionization in the dynamical expansion of strongly interacting bosons. However, the measures beyond the one-body level are able to distinguish strongly interacting bosons from noninteracting fermions in the dynamics. To understand how the two systems reach close proximity at the onset of fermionization, we extend all the measures in the two-body level. The two-body momentum distribution clearly distinguish the two systems in the dynamical evolution. The measures of relative entropies using two-body momentum density also quantitatively exhibit the distinction between the two systems. The two-body local and nonlocal correlations also conclude the same physics. Additionally, we find that the interacting bosons exhibit very rich structure in the higher-body densities, whereas for the fermions three- and higher-body correlations are ideally zero. We also provide quantitative estimates of different measurable quantities for both the one- and two-body level, which can be validated in the recent experiments of the quasi-1D setup.

ACKNOWLEDGMENTS

B.C. and A.G. acknowledge funding from Fundação de Amparo á Pesquisa do Estado de São Paulo (FAPESP), Grant No. 2023/06550-4. A.G. also acknowledges funding from Conselho Nacional de Desenvolvimento Científico e Tecnológico (CNPq), Grant No. 306219/2022-0. We are thankful to Rhombik Roy for helpful discussion.

[1] E. H. Lieb and W. Liniger, Exact analysis of an interacting Bose gas. I. The general solution and the ground state, Phys. Rev. **130**, 1605 (1963).
[2] E. H. Lieb, Exact analysis of an interacting Bose gas. II. The excitation spectrum, Phys. Rev. **130**, 1616 (1963).
[3] F. Dalfovo, S. Giorgini, L. P. Pitaevskii, and S. Stringari, Theory of Bose-Einstein condensation in trapped gases, Rev. Mod. Phys. **71**, 463 (1999).
[4] D. M. Gangardt and G. V. Shlyapnikov, Stability and phase coherence of trapped 1D Bose gases, Phys. Rev. Lett. **90**, 010401 (2003).
[5] C. Menotti and S. Stringari, Collective oscillations of a one-dimensional trapped Bose-Einstein gas, Phys. Rev. A **66**, 043610 (2002).
[6] D. S. Petrov, G. V. Shlyapnikov, and J. T. M. Walraven, Regimes of quantum degeneracy in trapped 1D gases, Phys. Rev. Lett. **85**, 3745 (2000).
[7] M. D. Girardeau, Permutation symmetry of many-particle wave functions, Phys. Rev. **139**, B500 (1965).
[8] D. M. Gangardt and G. V. Shlyapnikov, Local correlations in a strongly interacting one-dimensional Bose gas, New J. Phys. **5**, 79 (2003).

[9] A. Minguzzi and D. M. Gangardt, Exact coherent states of a harmonically confined Tonks-Girardeau gas, Phys. Rev. Lett. **94**, 240404 (2005).

[10] M. Rigol and A. Muramatsu, Fermionization in an expanding 1D gas of hard-core bosons, Phys. Rev. Lett. **94**, 240403 (2005).

[11] D. Muth, B. Schmidt, and M. Fleischhauer, Fermionization dynamics of a strongly interacting one-dimensional Bose gas after an interaction quench, New J. Phys. **12**, 083065 (2010).

[12] V. I. Yukalov and M. D. Girardeau, Fermi-Bose mapping for one-dimensional Bose gases, Laser Phys. Lett. **2**, 375 (2005).

[13] J. M. Wilson, N. Malvania, Y. Le, Y. Zhang, M. Rigol, and D. S. Weiss, Observation of dynamical fermionization, Science **367**, 1461 (2020).

[14] D. M. Gangardt and M. Pustilnik, Correlations in an expanding gas of hard-core bosons, Phys. Rev. A **77**, 041604(R) (2008).

[15] A. I. Streltsov, O. E. Alon, and L. S. Cederbaum, General variational many-body theory with complete self-consistency for trapped bosonic systems, Phys. Rev. A **73**, 063626 (2006).

[16] A. I. Streltsov, O. E. Alon, and L. S. Cederbaum, Role of excited states in the splitting of a trapped interacting Bose-Einstein condensate by a time-dependent barrier, Phys. Rev. Lett. **99**, 030402 (2007).

[17] O. E. Alon, A. I. Streltsov, and L. S. Cederbaum, Unified view on multiconfigurational time propagation for systems consisting of identical particles, J. Chem. Phys. **127**, 154103 (2007).

[18] O. E. Alon, A. I. Streltsov, and L. S. Cederbaum, Multiconfigurational time-dependent Hartree method for bosons: Many-body dynamics of bosonic systems, Phys. Rev. A **77**, 033613 (2008).

[19] A. U. J. Lode, Multiconfigurational time-dependent Hartree method for bosons with internal degrees of freedom: Theory and composite fragmentation of multicomponent Bose-Einstein condensates, Phys. Rev. A **93**, 063601 (2016).

[20] E. Fasshauer and A. U. J. Lode, Multiconfigurational time-dependent Hartree method for fermions: Implementation, exactness, and few-fermion tunneling to open space, Phys. Rev. A **93**, 033635 (2016).

[21] A. U. J. Lode, C. Lévêque, L. B. Madsen, A. I. Streltsov, and O. E. Alon, Colloquium: Multiconfigurational time-dependent Hartree approaches for indistinguishable particles, Rev. Mod. Phys. **92**, 011001 (2020).

[22] S. Kvaal, Variational formulations of the coupled-cluster method in quantum chemistry, Mol. Phys. **111**, 1100 (2013).

[23] P. Kramer and M. Saraceno, *Geometry of the Time-Dependent Variational Principle in Quantum Mechanics* (Springer Berlin, Heidelberg, 1981).

[24] A. D. McLachlan, A variational solution of the time-dependent Schrödinger equation, Mol. Phys. **8**, 39 (1964).

[25] L. Cao, V. Bolsinger, S. I. Mistakidis, G. M. Koutentakis, S. Krönke, J. M. Schurer, and P. Schmelcher, A unified ab initio approach to the correlated quantum dynamics of ultracold fermionic and bosonic mixtures, J. Chem. Phys. **147**, 044106 (2017).

[26] R. Lin, C. Georges, J. Klinder, P. Molignini, M. Büttner, A. U. J. Lode, R. Chitra, A. Hemmerich, and H. Keßler, Mott transition in a cavity-boson system: A quantitative comparison between theory and experiment, SciPost Phys. **11**, 030 (2021).

[27] J. H. V. Nguyen, M. C. Tsatsos, D. Luo, A. U. J. Lode, G. D. Telles, V. S. Bagnato, and R. G. Hulet, Parametric excitation of a Bose-Einstein condensate: From Faraday waves to granulation, Phys. Rev. X **9**, 011052 (2019).

[28] A. U. J. Lode, K. Sakmann, O. E. Alon, L. S. Cederbaum, and A. I. Streltsov, Numerically exact quantum dynamics of bosons with time-dependent interactions of harmonic type, Phys. Rev. A **86**, 063606 (2012).

[29] A. U. J. Lode, B. Chakrabarti, and V. K. B. Kota, Many-body entropies, correlations, and emergence of statistical relaxation in interaction quench dynamics of ultracold bosons, Phys. Rev. A **92**, 033622 (2015).

[30] S. Bera, R. Roy, A. Gammal, B. Chakrabarti, and B. Chatterjee, Probing relaxation dynamics of a few strongly correlated bosons in a 1D triple well optical lattice, J. Phys. B: At. Mol. Opt. Phys. **52**, 215303 (2019).

[31] R. Roy, A. Gammal, M. C. Tsatsos, B. Chatterjee, B. Chakrabarti, and A. U. J. Lode, Phases, many-body entropy measures, and coherence of interacting bosons in optical lattices, Phys. Rev. A **97**, 043625 (2018).

[32] R. Roy, C. Lévâque, A. U. J. Lode, A. Gammal, and B. Chakrabarti, Fidelity and entropy production in quench dynamics of interacting bosons in an optical lattice, Quantum Rep. **1**, 304 (2019).

[33] R. Roy, B. Chakrabarti, and A. Trombettoni, Quantum dynamics of few dipolar bosons in a double-well potential, Eur. Phys. J. D **76**, 215303 (2022).

[34] R. Lin, P. Molignini, L. Papariello, M. C. Tsatsos, C. Lévêque, S. E. Weiner, E. Fasshauer, and R. Chitra, MCTDH-X: The multiconfigurational time-dependent Hartree method for indistinguishable particles software, Quantum Sci. Technol. **5**, 024004 (2020).

[35] A. U. J. Lode, M. C. Tsatsos, E. Fasshauer, S. E. Weiner, R. Lin, L. Papariello, P. Molignini, C. Lévêque, M. Büttner, J. Xiang, S. Dutta, and Y. Bilinskaya, MCTDH-X: The multiconfigurational time-dependent Hartree method for indistinguishable particles software (2024).

[36] K. Sakmann, A. I. Streltsov, O. E. Alon, and L. S. Cederbaum, Reduced density matrices and coherence of trapped interacting bosons, Phys. Rev. A **78**, 023615 (2008).

[37] S. J. C. Salazar, H. G. Laguna, V. Prasad, and R. P. Sagar, Shannon-information entropy sum in the confined hydrogenic atom, Int. J. Quantum Chem. **120**, e26188 (2020).

[38] N. Aquino, A. Flores-Riveros, and J. Rivas-Silva, Shannon and Fisher entropies for a hydrogen atom under soft spherical confinement, Phys. Lett. A **377**, 2062 (2013).

[39] L. G. Jiao, L. R. Zan, Y. Z. Zhang, and Y. K. Ho, Benchmark values of Shannon entropy for spherically confined hydrogen atom, Int. J. Quantum Chem. **117**, e25375. (2017).

[40] K. D. Sen, Characteristic features of Shannon information entropy of confined atoms, J. Chem. Phys. **123**, 074110 (2005).

[41] T. Sriraman, B. Chakrabarti, A. Trombettoni, and P. Muruganandam, Characteristic features of the Shannon information entropy of dipolar Bose-Einstein condensates, J. Chem. Phys. **147**, 044304 (2017).

[42] R. Roy, B. Chakrabarti, N. D. Chavda, and M. L. Lekala, Information theoretic measures for interacting bosons in optical lattice, Phys. Rev. E **107**, 024119 (2023).

[43] J.-G. Baak and U. R. Fischer, Classical and quantum metrology of the Lieb-Liniger model, Phys. Rev. A **106**, 062442 (2022).

[44] S. Kullback, *Statistics and Information Theory* (Wiley, New York, 1959).

[45] C. Rao, *Differential Geometry in Statistical Interference*, IMS-Lecture Notes (Wiley, New York, 1987), Vol. 10, p. 217.

[46] S. Baratpour and R. A. Habibi, Testing goodness-of-fit for exponential distribution based on cumulative residual entropy, Commun. Stat. - Theory Methods **41**, 1387 (2012).

[47] T. M. Cover and J. A. Thomas, *Elements of Information Theory* (John Wiley and Sons, Hoboken, 2006).

[48] J. Lin, Divergence measures based on the Shannon entropy, IEEE Trans. Inf. Theory **37**, 145 (1991).

[49] A. Majtey, P. W. Lamberti, M. T. Martin, and A. Plastino, Wootters' distance revisited: A new distinguishability criterium, Eur. Phys. J. D **32**, 413 (2005).